Supplementary Information

Mechanistic Insight of $KBiQ_2$ (Q = S, Se) using Panoramic Synthesis towards Synthesis-by-Design

Rebecca McClain,[1] Christos D. Malliakas,[1] Jiahong Shen,[2] Jiangang He,[2] Chris Wolverton,[2] Gabriela B. González,[3] and Mercouri G. Kanatzidis[1]

[1]*Department of Chemistry, Northwestern University, Evanston, Illinois 60208, United States*

[2]*Department of Materials Science and Engineering, Northwestern University, Evanston, Illinois 60208, United States*

[3]*Department of Physics, DePaul University, Chicago, Illinois, 60614 United States*

List of Figures

List of Tables

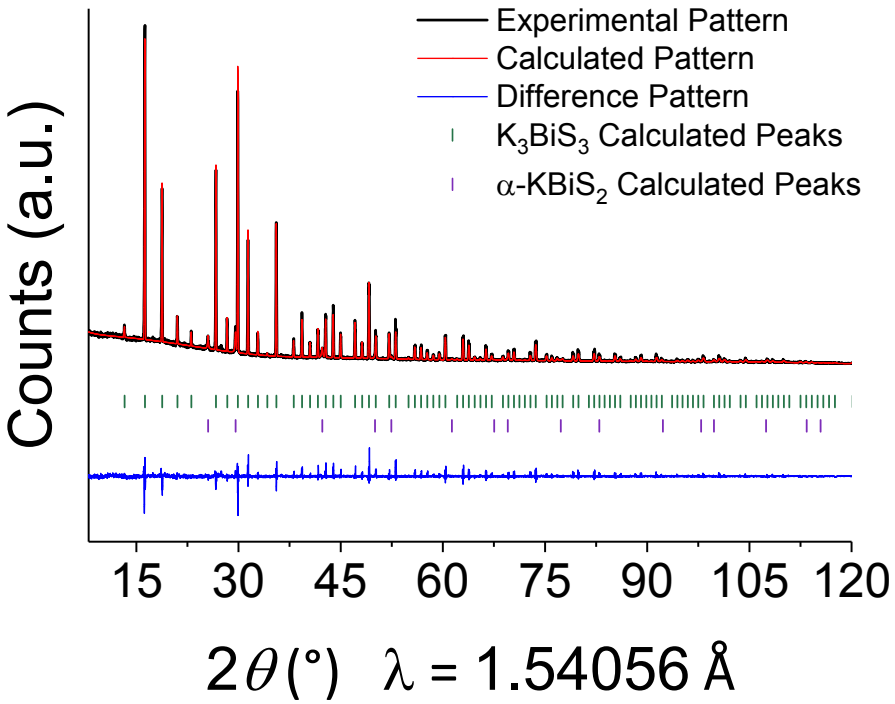

Figure S1: Structure solution for K_3BiS_3 from powder x-ray diffraction data.

Structure for K_3BiS_3 was solved from PXRD data collected on a STOE STADI P (Cu Kα1 radiation) using Rietveld refinement. A 7.7(2) wt% impurity of α-$KBiS_2$ was calculated in the sample.

Table S1. Crystal data and structure refinement for K_3BiS_3 at 298 K.

Empirical formula	K3 Bi1 S3
Formula weight	422.5
Temperature	298 K
Wavelength	1.54056 Å
Crystal system	cubic
Space group	$P2_13$
Unit cell dimensions	a = 9.44252(14) Å, α = 90°
	b = 9.44252(14) Å, β = 90°
	c = 9.44252(14) Å, γ = 90°
Volume	841.91(2) $Å^3$
Z	4
Density (calculated)	3.3329 g/cm^3
Absorption coefficient	60.678 mm^{-1}
F(000)	64
2θ range for data collection	3.000 to 124.680° [Step 0.015°]
Refinement method	Rietveld Refinement
Constraints / restraints / parameters	0 / 0 / 42
Goodness-of-fit	1.53
Profile R indices	$R_p = 0.0886$, $wR_p = 0.1362$
Final Bragg R indices [2σ]	$R_{Bragg} = 0.0586$, $wR_{Bragg} = 0.0631$
Bragg R indices [all data]	$R_{all} = 0.0663$, $wR_{all} = 0.0635$
Largest diff. peak and hole	0.72 and -1.83 $e \cdot Å^{-3}$

$R = \Sigma||F_o|-|F_c|| / \Sigma|F_o|$, $wR = \{\Sigma[w(|F_o|^2 - |F_c|^2)^2] / \Sigma[w(|F_o|^4)]\}^{1/2}$

Table S2: Atomic coordinates (x10^4) and equivalent isotropic displacement parameters (Å^{2}x10^3) for K_3BiS_3 at 298 K with estimated standard deviations in parentheses.

Label	x	y	z	Occupancy	U_{eq}*
K(1)	614(12)	614(12)	614(12)	1	88(3)
K(2)	5777(12)	5777(12)	5777(12)	1	146(6)
K(3)	8221(11)	8221(11)	8221(11)	1	159(5)
Bi(1)	2842(2)	2842(2)	2842(2)	1	108(1)
S(1)	412(11)	2612(11)	3524(9)	1	106(5)

*U_{eq} is defined as one third of the trace of the orthogonalized U_{ij} tensor.

Table S3: Selected bond lengths [Å] for K_3BiS_3 at 298 K with estimated standard deviations in parentheses.

Label	Distances
K(1)-K(2)	3.655(16)
K(1)-K(3)	3.914(16)
K(1)-K(3)	4.515(15)
K(1)-Bi(1)	3.645(11)
K(1)-Bi(1)	4.430(11)
K(1)-S(1)	3.338(14)
K(1)-S(1)	3.105(15)
K(2)-K(3)	3.997(15)
K(2)-K(3)	4.580(15)
K(2)-Bi(1)	4.145(11)
K(2)-S(1)	3.210(14)
K(2)-S(1)	3.285(15)
K(3)-Bi(1)	3.867(10)
K(3)-S(1)	3.531 (14)
K(3)-S(1)	3.383(14)
Bi(1)-S(1)	2.393(10)

Symmetry transformations used to generate equivalent atoms:

(1) -x+1/2,-y+1,z-1/2 (2) -x+1,y-1/2,-z+1/2 (3) x-1/2,-y+1/2,-z+1 (4) x-1,y-1,z-1 (5) -x+1/2,-y,z-1/2 (6) -x,y-1/2,-z+1/2 (7) x-1/2,-y+1/2,-z (8) z,x,y (9) -z+1/2,-x,y-1/2 (10) y,z,x (11) y-1/2,-z+1/2,-x (12) -x+3/2,-y+1,z-1/2 (13) -x+1,y-1/2,-z+3/2 (14) x-1/2,-y+3/2,-z+1 (15) -x+1/2,-y+1,z+1/2 (16) -x+1,y+1/2,-z+1/2 (17) x+1/2,-y+1/2,-z+1 (18) z+1/2,-x+1/2,-y+1 (19) -z+1,x+1/2,-y+1/2 (20) -y+1,z+1/2,-x+1/2 (21) -y+1/2,-z+1,x+1/2 (22) -x+3/2,-y+1,z+1/2 (23) -x+1,y+1/2,-z+3/2 (24) x+1/2,-y+3/2,-z+1 (25) -z+3/2,-x+1,y+1/2 (26) y+1/2,-z+3/2,-x+1 (27) x+1,y+1,z+1 (28) -x+1/2,-y,z+1/2 (29) -x,y+1/2,-z+1/2 (30) x+1/2,-y+1/2,-z

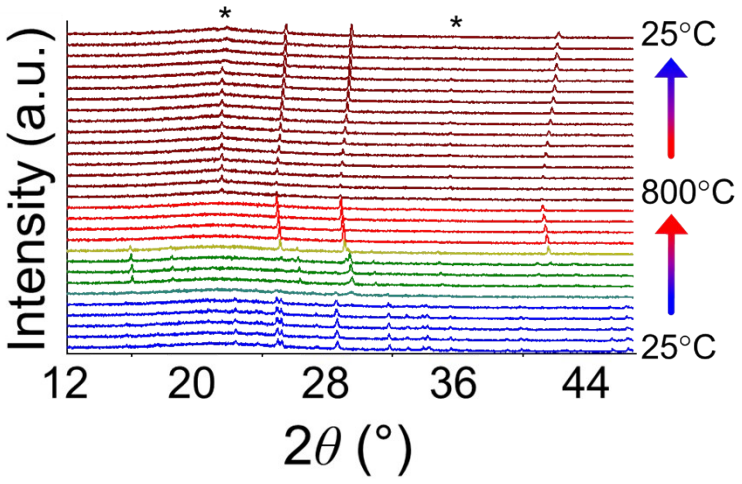

Figure S2: Overlaid diffraction patterns of 1.5 K2S + 1 Bi2S3 panoramic synthesis.

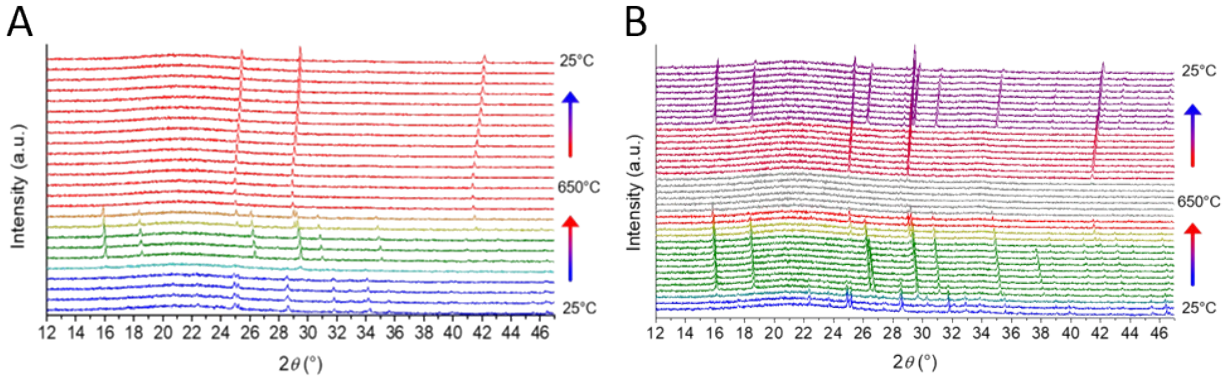

Figure S3: (a) Panoramic syntheses for 2 K_2S : 1 Bi_2S_3. (b) Panoramic synthesis for 5 K_2S : 1 Bi_2S_3. In this reaction, K_3BiS_3 appears earlier in the reaction (shown in green) and also as a final product with $KBiS_2$ (purple). The regime where materials are in a melt are shown in grey.

To study the influence of increased amounts of K_2S on the formation of $KBiS_2$ and investigate if additional potassium-rich phases exist, the amount of K_2S relative to Bi_2S_3 was

increased. These reactions, and subsequent reactions, were conducted at a maximum temperature of 650°C to avoid the crystallization of the SiO_2 spacer to cristobalite. With an increase in the K_2S, the 2 K_2S : 1 Bi_2S_3 reaction features a pathway is similar to that of the 1.5:1 ratio, as shown in Figure S3a. K_3BiS_3 forms at ca. 270°C and disappears at ca. 585°C, as indicated by the green patterns; $KBiS_2$ evolves at ca. 465°C, as denoted by the red patterns. However, when the amount of K_2S is further increased to a 5:1 ratio, the K_3BiS_3 appears at a lower temperature and as a final product.

The increased ratio of K_2S in the 5:1 ratio manifests in different behavior of the K-Bi-S system. The the crystallization of the intermediate formed at a lower temperature, the intermediate appeared as a final product, and $KBiS_2$ melted at a temperature lower than 650°C. K_3BiS_3 crystallized at 180°C and $KBiS_2$ emerges at 420°C, as shown in green and red, respectively, in Figure S3b. In this ratio, K_3BiS_3 also appears as a final product after recrystallizing at 375°C upon cooling. The increased concentration of K_2S in this reaction appears to stabilize K_3BiS_3 at ambient temperature, as it is present as a final product in the 5:1 ratio. It is unclear if the concentration gradient drives the formation to a lower reaction temperature or if, for example, the excess of K_2S stabilizes the intermediate phase thereby enabling a lower reaction temperature. Additional characterization of the local structure, such as Pair Distribution Function, would elucidate if the earlier occurrence is a result of surface stabilizing effects. In this reaction, K_3BiS_3 and $KBiS_2$ persist until melting by 600°C; this is the first instance of in this work that $KBiS_2$ melts below 750°C. Using in-situ techniques, we have discovered that the increased ratio of K_2S lowers the formation temperature for a key intermediate phase, promotes the melting of $KBiS_2$, and manifests in the formation of the intermediate phase other not observed at ambient temperature.

Table S4: Crystal data and structure refinement for β-$KBiS_2$ at 293 K.

Empirical formula	K Bi S2
Formula weight	312.2
Temperature	293 K
Wavelength	0.45777 Å
Crystal system	trigonal
Space group	R-3m
Unit cell dimensions	a = 4.12983(3) Å, α = 90° b = 4.12983(3) Å, β = 90° c = 22.09484(17) Å, γ = 120°
Volume	326.351(4) $Å^3$
Z	3
Density (calculated)	4.7656 g/cm^3
Absorption coefficient	13.565 mm^{-1}
F(000)	402
2θ range for data collection	2.004 to 29.997° [Step 0.001°]
Refinement method	Rietveld
Constraints / restraints / parameters	0 / 0 / 25
Goodness-of-fit	1.21
Profile R indices	$R_p = 0.1286$, $wR_p = 0.1662$
Final Bragg R indices [2σ]	$R_{Bragg} = 0.0183$, $wR_{Bragg} = 0.0220$
Bragg R indices [all data]	$R_{all} = 0.0183$, $wR_{all} = 0.0220$
Largest diff. peak and hole	0.63 and -0.68 $e \cdot Å^{-3}$

$R = \Sigma||F_o|-|F_c|| / \Sigma|F_o|$, $wR = \{\Sigma[w(|F_o|^2 - |F_c|^2)^2] / \Sigma[w(|F_o|^4)]\}^{1/2}$

Table S5: Atomic coordinates (x10^4) and equivalent isotropic displacement parameters (Å^{2}x10^3) for β-KBiS$_2$ at 293 K with estimated standard deviations in parentheses.

Label	x	y	z	Occupancy	U_{eq}*
Bi(1)	0	0	0	1	39(1)
K(1)	3333.33	6666.67	1666.67	1	34(1)
S(1)	-3333.33	3333.33	710(1)	1	35(1)

*U_{eq} is defined as one third of the trace of the orthogonalized U_{ij} tensor.

Table S6: Anisotropic displacement parameters (Å^{2}x10^3) for β-KBiS$_2$ at 293 K with estimated standard deviations in parentheses.

Label	U_{11}	U_{22}	U_{33}	U_{12}	U_{13}	U_{23}
Bi(1)	38(1)	38(1)	41(1)	19(1)	0	0
K(1)	37(1)	37(1)	27(2)	19(1)	0	0
S(1)	37(1)	37(1)	31(2)	18(1)	0	0

The anisotropic displacement factor exponent takes the form: $-2\pi^2[h^2a^{*2}U_{11} + ... + 2hka^*b^*U_{12}]$.

Table S7: Selected bond lengths [Å] for β-KBiS$_2$ at 293 K with estimated standard deviations in parentheses.

Label	Distances
Bi(1)-K(1)	4.38700(5)
Bi(1)-S(1)	2.8540(10)
K(1)-K(1)	4.12983(5)
K(1)-S(1)	3.1865(12)

Symmetry transformations used to generate equivalent atoms:

(1) x-1,y-1,z (2) x,y-1,z (3) x+1/3,y+2/3,z+2/3 (4) x+1/3,y+2/3,z+2/3 (5) x+1/3,y+2/3,z+2/3 (6) x+1,y,z (7) y-1,x,-z (8) y,x,-z (9) y,x+1,-z (10) x-1,y,z (11) x,y+1,z (12) x+1,y+1,z (13) y+2/3,x+1/3,-z+1/3 (14) y+2/3,x+1/3,-z+1/3 (15) y+2/3,x+1/3,-z+1/3 (16) x+2/3,y+1/3,z+1/3 (17) x+2/3,y+1/3,z+1/3 (18) x+2/3,y+1/3,z+1/3

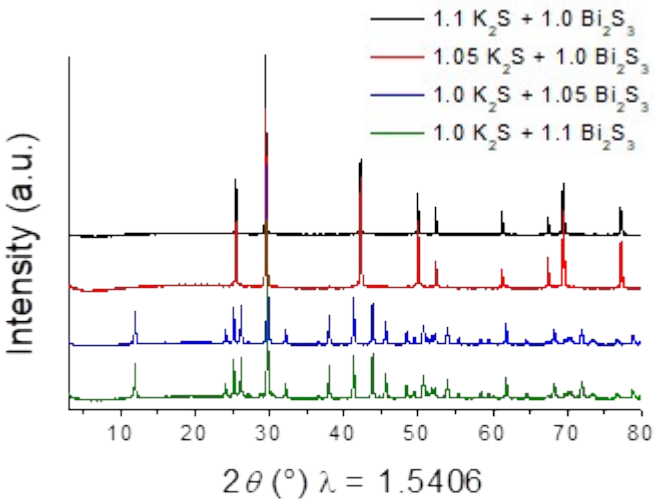

Figure S4: Reactions to test boundary of ordered vs disordered rocksalt formation for $KBiS_2$. Stoichiometric ratio yielded the ordered phase, while a 5% excess yielded disordered phase.

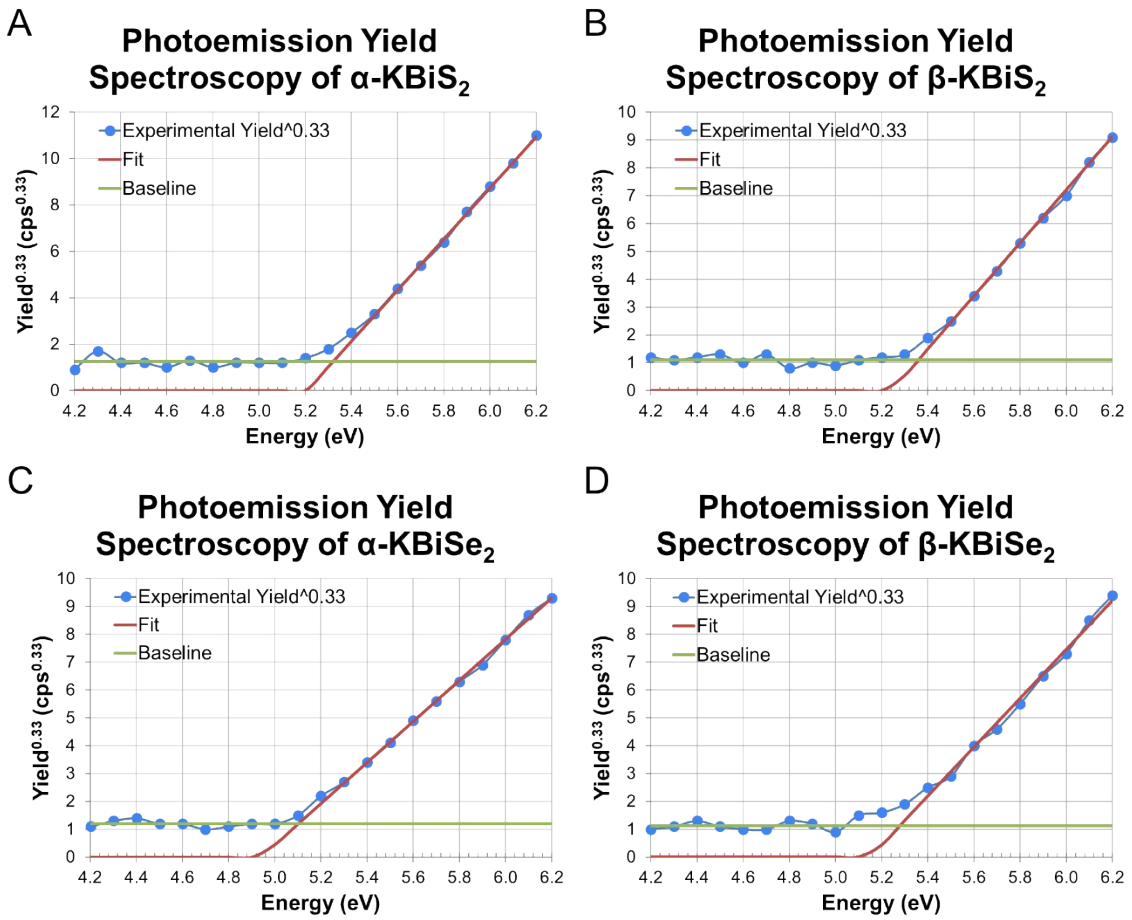

Figure S5: Photoemissions yield spectroscopy in air using a Kelvin Probe for (a) α-$KBiS_2$, (b) β-$KBiS_2$, (c) α-$KBiSe_2$ and (d) β-$KBiSe_2$.

Energy of valence band maxima is determined from the intersection of the baseline and fit line for the respective spectrum. Experimental energies of valence band maxima are shown in Table S11.

Table S8: Table of valence band maxima, conduction band minima, and band gap energies.

	Valence Band Maxima (eV)	Conduction Band Minima (eV)	Band Gap (eV)
α-$KBiS_2$	5.32	4.09	1.23
β-$KBiS_2$	5.36	3.81	1.55
α-$KBiSe_2$	5.10	4.26	0.84
β-$KBiSe_2$	5.28	4.19	1.09
Si	4.60	3.5	1.1
CdTe	4.95	3.5	1.5
a-TiO_2	5.16	2.0	3.2
$MAPbI_3$	5.44	3.92	1.52

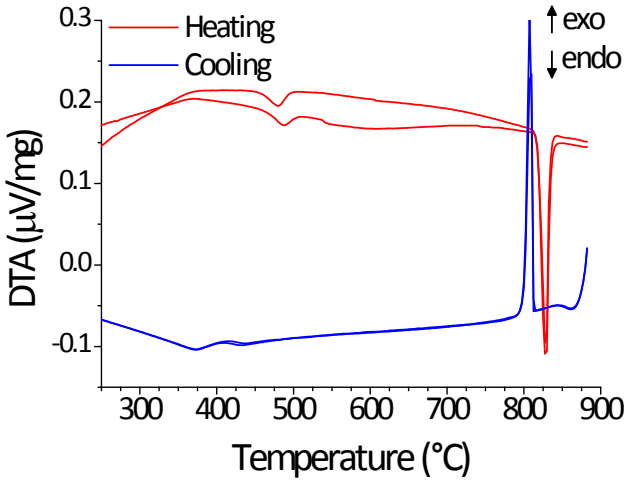

Figure S6: β-$KBiS_2$ thermal analysis.

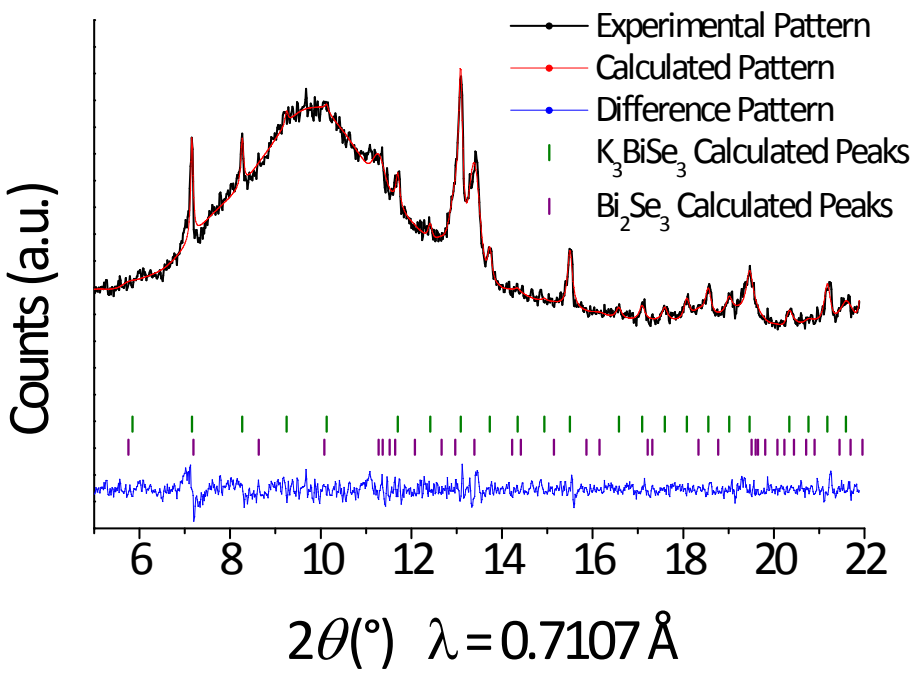

Figure S7: Le Bail refinement for PXRD collected at 195°C during K_2Se + Bi_2Se_3 panoramic synthesis. The lattice constant for K_3BiSe_3 expands to 9.8590(7) Å at 195°C. As shown by this refinement, Bi_2Se_3 persists at this temperature.

Table S9: Crystal data and structure refinement for β-$KBiSe_2$ at 298 K.

Empirical formula	K1 Bi1 Se2
Formula weight	406
Temperature	298 K
Wavelength	0.41283 Å
Crystal system	trigonal
Space group	R -3 m
Unit cell dimensions	a = 4.264423(14) Å, α = 90° b = 4.264423(14) Å, β = 90° c = 23.02901(14) Å, γ = 120°
Volume	362.682(3) $Å^3$
Z	3
Density (calculated)	5.5766 g/cm^3
Absorption coefficient	12.726 mm^{-1}
F(000)	510
2θ range for data collection	0.500 to 27.581° [Step 0.001°]
Refinement method	Rietveld Refinement
Constraints / restraints / parameters	0 / 0 / 26
Goodness-of-fit	1.10
Profile R indices	$R_p = 0.1383$, $wR_p = 0.1762$
Final Bragg R indices [3σ]	$R_{Bragg} = 0.0263$, $wR_{Bragg} = 0.0287$
Bragg R indices [all data]	$R_{all} = 0.0269$, wR_{all} = N/A
Largest diff. peak and hole	1.04 and -3.45 e·$Å^{-3}$

$R = \Sigma||F_o|-|F_c|| / \Sigma|F_o|$, $wR = \{\Sigma[w(|F_o|^2 - |F_c|^2)^2] / \Sigma[w(|F_o|^4)]\}^{1/2}$

Table S10: Atomic coordinates (x10^4) and equivalent isotropic displacement parameters ($Å^2$x10^3) for β-$KBiSe_2$ at 298 K with estimated standard deviations in parentheses.

Label	x	y	z	Occupancy	U_{eq}*
Bi(1)	3333.33	6666.67	1666.67	1	21(1)
K(1)	0	0	0	1	18(2)
Se(1)	0	0	2385(1)	1	16(1)

*U_{eq} is defined as one third of the trace of the orthogonalized U_{ij} tensor.

Table S11: Anisotropic displacement parameters ($Å^2x10^3$) for β-$KBiSe_2$ at 298 K with estimated standard deviations in parentheses.

Label	U_{11}	U_{22}	U_{33}	U_{12}	U_{13}	U_{23}
Bi(1)	19(1)	19(1)	25(1)	9(1)	0	0
K(1)	22(2)	22(2)	11(2)	11(1)	0	0
Se(1)	17(1)	17(1)	14(1)	9(1)	0	0

The anisotropic displacement factor exponent takes the form: $-2\pi^2[h^2a^{*2}U_{11} + ... + 2hka^*b^*U_{12}]$.

Table S12: Bond lengths [Å] for β-$KBiSe_2$ at 298 K with estimated standard deviations in parentheses.

Label	Distances
Bi(1)-K(1)	4.55997(4)
Bi(1)-Se(1)	2.9664 (6)
K(1)-K(1)	4.26442(4)
K(1)-Se(1)	3.2908(7)

Symmetry transformations used to generate equivalent atoms:

(1) x,y+1,z (2) x+1,y+1,z (3) x+2/3,y+1/3,z+1/3 (4) x+2/3,y+1/3,z+1/3 (5) x+2/3,y+1/3,z+1/3 (6) y+2/3,x+1/3,-z+1/3 (7) y+2/3,x+1/3,-z+1/3 (8) y+2/3,x+1/3,-z+1/3 (9) x-1,y-1,z (10) x-1,y,z (11) x,y-1,z (12) x+1,y,z (13) x+1/3,y+2/3,z+2/3 (14) x+1/3,y+2/3,z+2/3 (15) x+1/3,y+2/3,z+2/3 (16) y+2/3,x+1/3,-z+1/3 (17) x+1/3,y+2/3,z+2/3 (18) x+2/3,y+1/3,z+1/3

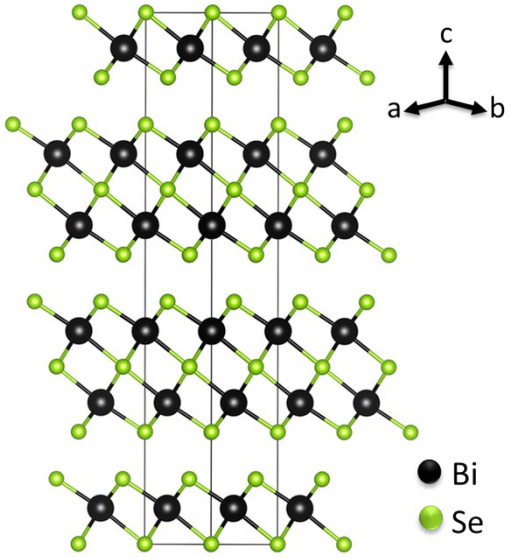

Figure S8: Extended structure of Bi_2Se_3.

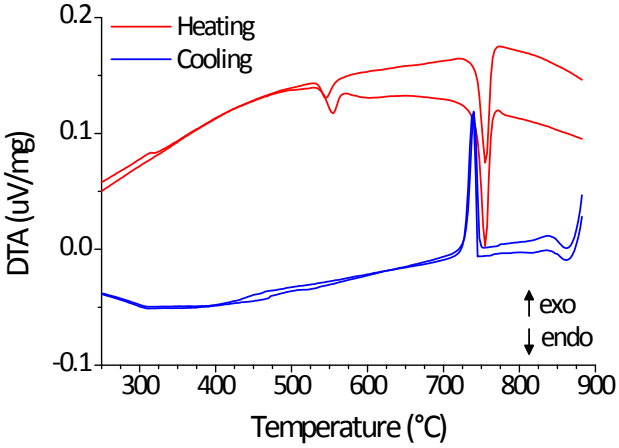

Figure S9: β-$KBiSe_2$ thermal analysis.

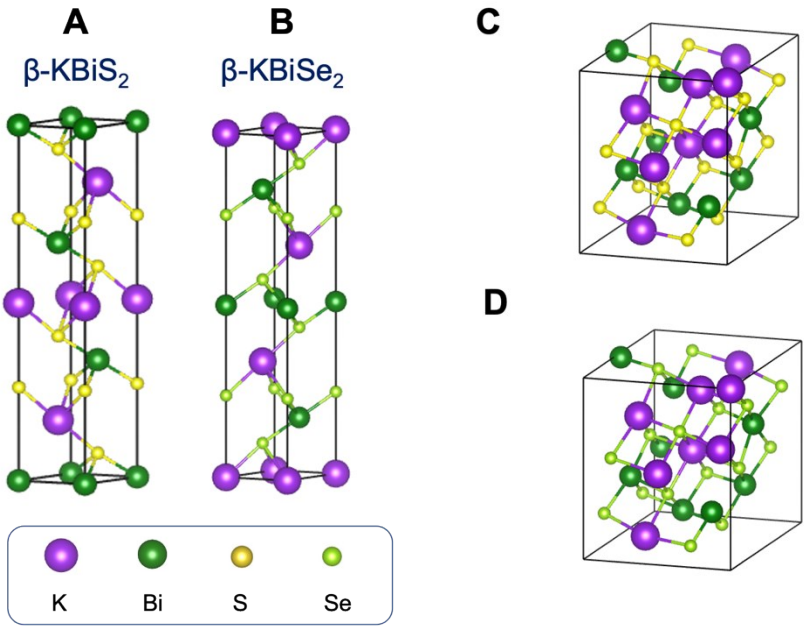

Figure S10: The crystal structures used in DFT calculations of (a) β-$KBiS_2$, (b) β-$KBiSe_2$, (c) α-$KBiS_2$ and (d) α-$KBiSe_2$.

The β-$KBiQ_2$ has a $R\bar{3}m$ structure, which is an elongated rocksalt-structure in the [111] direction. The α-$KBiQ_2$ ($Fm\bar{3}m$) is generated by both SQS (for formation energy calculations) and supercells (for band structure calculations).

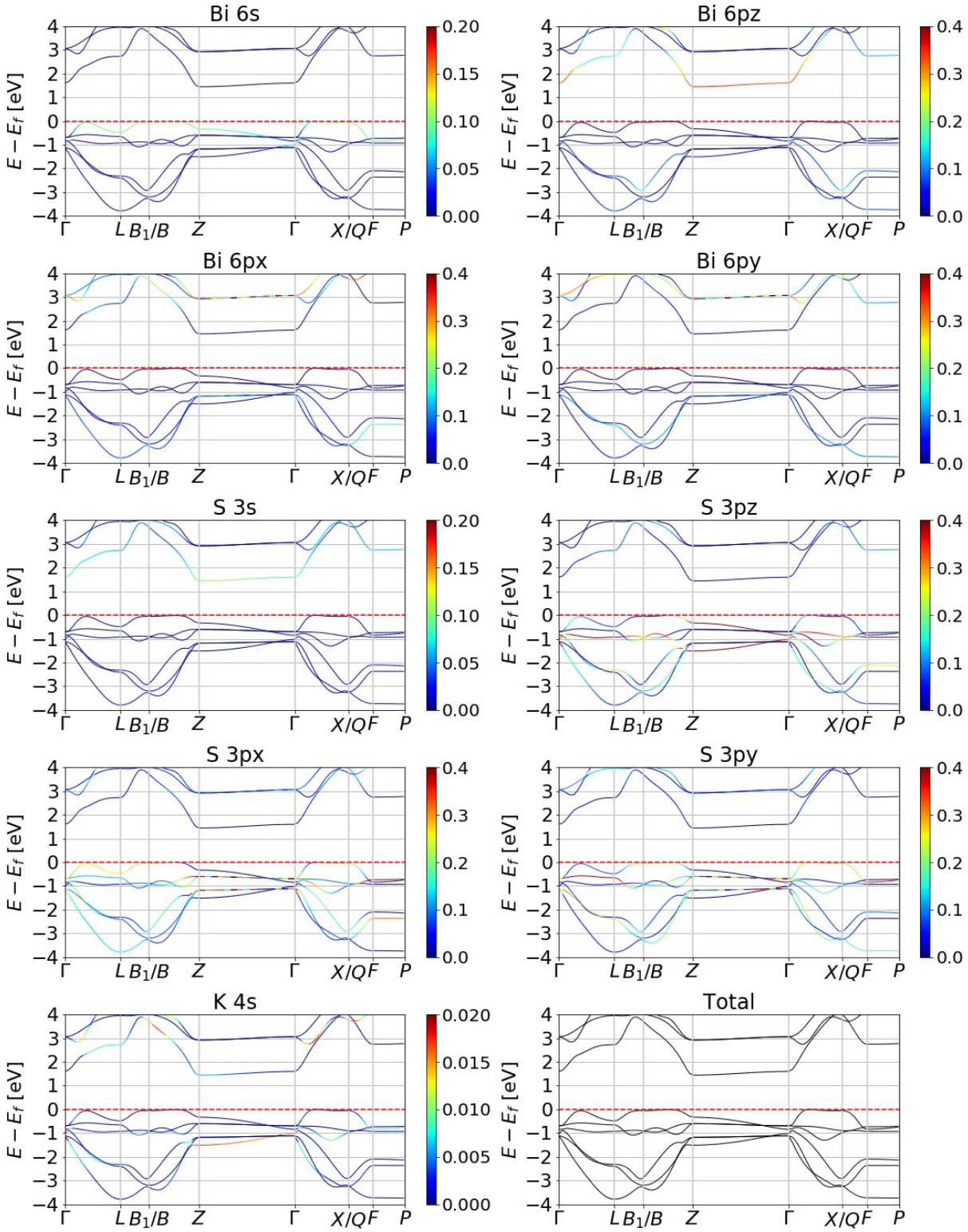

Figure S11: Orbital decomposed band structure, which shows the atomic orbital contribution to the β-$KBiS_2$ band structure.

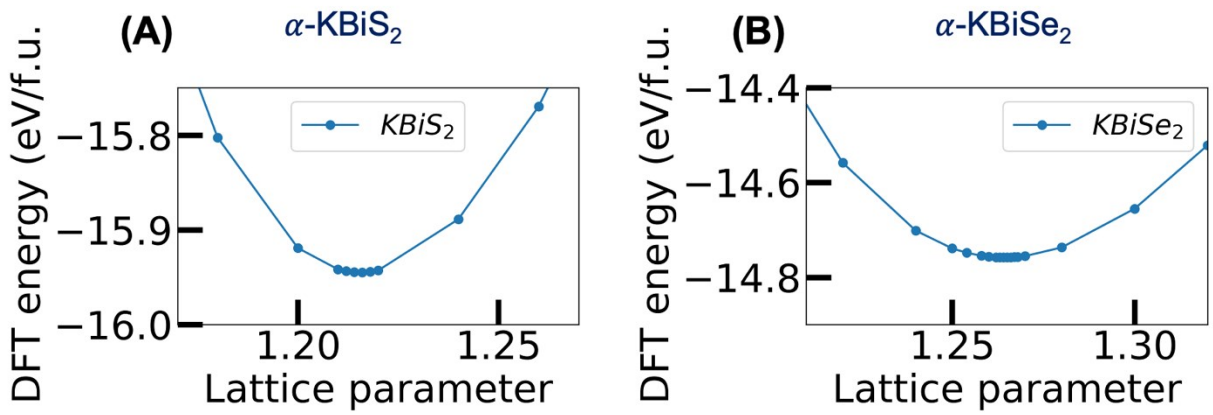

Figure S12: DFT total energies of (a) α-$KBiS_2$ and (b) α-$KBiSe_2$ as a function of lattice parameter scaled to the reference structure.

The lattice parameters of primitive rocksalt α-$KBiQ_2$ are determined by the lowest energy configurations as shown in Figure S12. The $2 \times 2 \times 2$ supercells are then generated using these lattice parameters and the lowest energy one is chosen from 10 randomly mixed cation-disordered supercells as the structures for α-$KBiQ_2$.

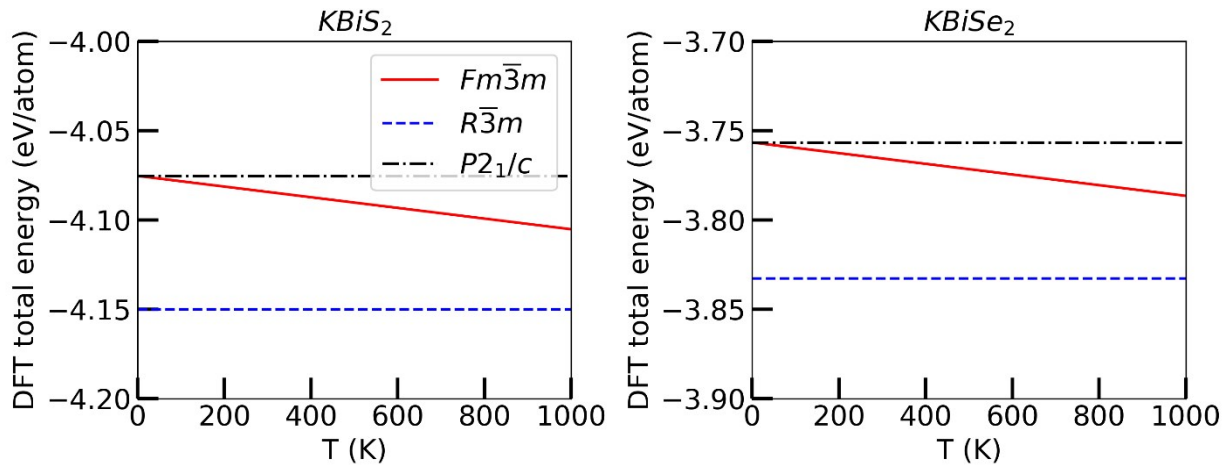

Figure S13: DFT mixing entropy calculations for the stability of $KBiQ_2$ (Q = S, Se) crystallized in the rocksalt ($Fm\bar{3}m$, red line), α-$NaFeO_2$ ($R\bar{3}m$, blue line), and $CsSbS_2$ ($P2_1/c$, black line) structure types at finite temperatures.

DFT mixing entropy calculations confirm the energetic stability of $KBiS_2$ and $KBiSe_2$ crystallizing in the α-$NaFeO_2$ ($R\bar{3}m$) structure type over the rocksalt and $CsSbS_2$ structure types. The calculations additionally highlight that the $KBiQ_2$ compositions are least stable in the monoclinic $CsSbS_2$ structure type compared to the $Fm\bar{3}m$ and $R\bar{3}m$ structures, thereby corroborating the experimental observation that $KBiQ_2$ does not crystallize in this monoclinic structure type.

Table S13: Energy differences (ΔE) in meV/atom between the $CsSbS_2$ ($P2_1/c$) and α-$NaFeO_2$ ($R\bar{3}m$) structure types for reported $ABiQ_2$ (A=Li, Na, K, Rb, Cs; Q=S, Se, Te) compounds, where $\Delta E = E_{P2_1/c} - E_{R\text{-}3m}$.

	Li	**Na**	**K**	**Rb**	**Cs**
S	14	18	75	46	10
Se	–	23	76	–	–
Te	28	28	–	–	–

The structures of $RbBiS_2$ ($R\bar{3}m$) and $CsBiS_2$ ($P2_1/c$) are used as prototypes for the $CsSbS_2$ ($P2_1/c$) and α-$NaFeO_2$ ($R\bar{3}m$) structure type while the SQS structure, as discussed in the main text, is used to simulate the disordered rocksalt structures.

Table S14: Fitted transition temperatures, in K, between the DFT-calculated ground state α-$NaFeO_2$ and the rocksalt structure types for all $ABiQ_2$ (A=Li, Na, K, Rb, Cs; Q=S, Se, Te) compounds.

	Li	**Na**	**K**	**Rb**	**Cs**
S	260 K	440 K	730 K	1220 K	690 K
Se	–	430 K	750 K	–	–
Te	260 K	400 K	–	–	–

The transition temperature between the α-$NaFeO_2$ and rocksalt structure types is proportional to the energy difference between the T = 0 K energy of the DFT-calculated ground state α-$NaFeO_2$ structure type and the T = 0 K energy of the SQS[68] rocksalt structures. By fitting the transition temperature of $KBiS_2$ (730K), we obtain the transition temperatures for all other compounds.

We note that the calculated transformation temperatures are fairly approximate, and should not be interpreted too quantitatively, but rather are only a guide of the order-disorder trends in these compounds. A more quantitative calculation of transformation temperature would involve determination of the configurational and vibrational entropy contributions, as shown by Hua *et al*.

Xia Hua, Shiqiang Hao, and Chris Wolverton, First-principles study of vibrational entropy effects on the PbTe-SrTe phase diagram, Phys. Rev. Materials 2, 095402.